



Original article

Isoxazole derivatives as potent transient receptor potential melastatin type 8 (TRPM8) agonists



Carmine Ostacolo^{a,*,1}, Paolo Ambrosino^{b,1}, Roberto Russo^{a,1}, Matteo Lo Monte^c,
 Maria Virginia Soldovieri^b, Sonia Laneri^a, Antonia Sacchi^a, Giulio Vistoli^c,
 Maurizio Tagliatela^{b,d,**}, Antonio Calignano^a

^a Department of Pharmacy, University of Naples Federico II, Via D. Montesano 49, 80131 Naples, Italy

^b Department of Medicine and Health Sciences, University of Molise, Via F. De Sanctis, 86100 Campobasso, Italy

^c Department of Pharmaceutical Science Piero Pratesi, University of Milan, Via L. Mangiagalli 25, 20133 Milan, Italy

^d Div. Pharmacology, Department of Neuroscience, University of Naples Federico II, Via Pansini 5, 80131 Naples, Italy

ARTICLE INFO

Article history:

Received 10 May 2013

Received in revised form

20 August 2013

Accepted 25 August 2013

Available online 20 September 2013

Keywords:

Transient receptor potential melastatin type-8 channels

Isoxazolylamine derivatives

Structure–activity relationship

Calcium imaging

Chronic constriction injury

ABSTRACT

Modulation of the transient receptor potential melastatin type-8 (TRPM8), the receptor for menthol acting as the major sensor for peripheral innocuous cool temperatures, has several important applications in pharmaceutical, food and cosmetic industries. In the present study, we designed 12 isoxazole derivatives and tested their pharmacological properties both in F11 sensory neurons *in vitro*, and in an *in vivo* model of cold allodynia. In F11 sensory neurons, single-cell Ca^{2+} -imaging experiments revealed that, when compared to menthol, some newly-synthesized compounds were up to 200-fold more potent, though none of them showed an increased efficacy. Some isoxazole derivatives potentiated allodynic responses elicited by acetone when administered to rats subjected to sciatic nerve ligation; when compared to menthol, these compounds were efficacious at earlier (0–2 min) but not later (7–9 or 14–16 min) time points. Docking experiments performed in a human TRPM8 receptor model revealed that newly-synthesized compounds might adopt two possible conformations, thereby allowing to distinguish “menthol-like” compounds (characterized by high efficacy/low potency), and “icillin-like” compounds (with high potency/low efficacy). Collectively, these data provide rationale structure–activity relationships for isoxazole derivatives acting as TRPM8 agonists, and suggest their potential usefulness for cold-evoked analgesia.

© 2013 Elsevier Masson SAS. All rights reserved.

1. Introduction

Since the days of Hippocrates and Galen [1,2], cooling agents have been successfully used to induce analgesia during traumatic injuries [3,4]. However, little is known about the molecular mechanisms underlying cooling-induced analgesia, albeit a number of cool-sensitive ion channels have been identified in

somatosensory afferents [5]. Among these, transient receptor potential melastatin type 8 (TRPM8) channels act as Ca^{2+} -permeable ligand-gated cation channels activated by chemical cooling agents (such as menthol) or by cold temperatures (<25 °C) [6–8]. Both peripheral and central activation of TRPM8 induces analgesic effects that specifically reverse the sensitization of the behavioral reflexes elicited by peripheral nerve injury [9]. These effects are produced in a range of very low concentrations of topically applied TRPM8 activators, whereas high concentrations of menthol were found to cause both cold and mechanical hyperalgesia in healthy volunteers [10,11]. These findings suggest the potential relevance of TRPM8 activators as therapeutic strategy for pain treatment [12–14].

Expression of TRPM8 also represents a prognostic marker and a therapeutic target in prostate cancer (PCa): indeed, the activation of TRPM8 receptors by menthol enhanced apoptosis of lymph node carcinoma of prostate cells (LNCaP) [15], pointing to a potential involvement of TRPM8 channels in cancer cell growth.

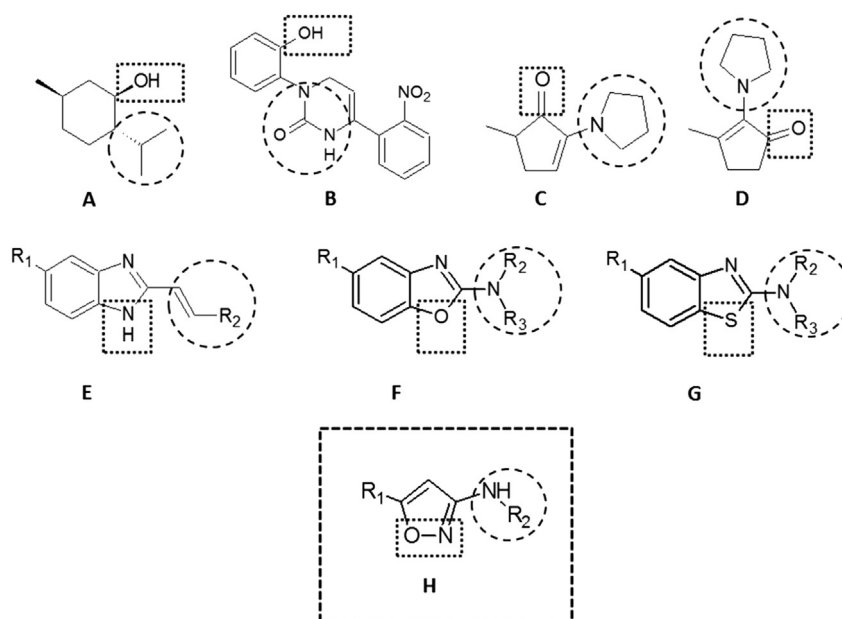
Abbreviations: TRPM8 channels, transient receptor potential melastatin type-8 channels; Ca^{2+} , calcium; GM, growth medium; DM, differentiation medium; DMEM, Dulbecco's modified Eagle's medium; FBS, fetal bovine serum; RT-PCR, reverse-transcription PCR; RT, room temperature; SAR, structure–activity relationship; CCI, chronic constriction injury.

* Corresponding author. Department of Pharmacy, University of Naples Federico II, Via D. Montesano 49, 80131 Naples, Italy. Tel.: +39 081 6788609.

** Corresponding author. Department of Medicine and Health Sciences, University of Molise, Via F. De Sanctis, 86100 Campobasso, Italy.

E-mail address: ostacolo@unina.it (C. Ostacolo).

¹ These authors equally contributed to this work.



Scheme 1. (A–G) Molecular structures of main TRPM8 modulators: menthol (A), icilin (B), α -ketoenamine (C and D), benzo-fused imidazole (E), oxazole (F) and thiazole derivatives (G). Generic structure of the newly synthesized compounds of the present study (H).

Given the potential role of TRPM8 agonists for the treatment of neuropathic pain conditions and cancer, increasing efforts in the last few years have been dedicated to the design of selective and potent TRPM8 ligands. To date, the most active cooling compound, icilin (Scheme 1B), is characterized by the presence of a central tetrahydropyrimidine-2-one ring substituted by a nitrophenyl and phenol moieties. Several other analogues, based on the tetrahydropyrimidine-2-one moiety, have been described and patented for their cooling activity [16].

The need for a heterocyclic ring to elicit efficient interactions with TRPM8 is also witnessed by the isolation of the potent cooling agents α -ketoenamine (Scheme 1C and D) from roast malt extract [17]; however, these molecules are penalized by their great instability to oxidation, probably related to the reactive enamine functional group. A similar instability was also found for a class of aminophenols synthesized as hybrid derivatives of icilin and ketoenamines [17]. Therefore, and in view of these stability issues, different heterocyclic moieties have been utilized as chemical scaffolds for the synthesis of new TRPM8 modulators; these include benzimidazole-based (Scheme 1E), as well as fused oxazole (Scheme 1F) and thiazole derivatives (Scheme 1G) [18,19]. In addition, aminoisoxazoles, in particular the 3-amino derivatives, are resistant to the typical degradation occurring to the isoxazole rings [20], and are suitable for simple and high-yield chemical derivatization of the amino group.

Substituted aminoisoxazole derivatives seem to include the minimum structural requirements for a TRPM8 ligand, as seen for menthol or icilin, such as hydrogen bonding groups, a compact (mainly cyclic) hydrocarbon backbone, a correct hydrophobic/hydrophilic balance with a $\log P$ range between 1 and 5, and a molecular weight in the range of 150–350 g/mol. Indeed, several structural similarities can be observed between the α -ketoenamine derivatives and the aminoisoxazoles (Scheme 1H) [21].

Based on these evidence and on the known SARs for menthol (Scheme 1A) and its analogues [21,22], in the present study we synthesized 12 new isoxazole derivatives (Scheme 2) carrying

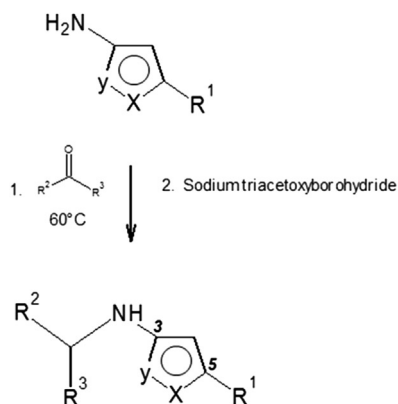
modifications on the isoxazole ring. These mainly involved the introduction of aminoaliphatic or aminoaromatic chains in position 3 and/or the introduction of a methyl group in position 5 of this scaffold ring.

When tested for their ability to trigger TRPM8-induced $[Ca^{2+}]_i$ responses in sensory neurons *in vitro*, some of these derivatives showed higher potency when compared to menthol. Thereafter, the most potent compounds were tested *in vivo* in an animal model of cold allodynia, where they showed strong and rapid, although short-lasting, allodynic responses. In order to identify the structural determinants for the higher potency of specific compounds, docking experiments were performed using the recently described TRPM8 model [23]. This approach revealed that the more potent compounds strongly stabilized the agonist binding site of TRPM8 receptors, favoring its active configuration. Altogether these results suggest that the newly-synthesized isoxazole derivatives act as potent TRPM8 modulators, and may represent promising drugs for pain treatment.

2. Results and discussion

2.1. Chemistry

Tested compounds were synthesized in a one-pot procedure, by reductive alkylation, using aldehyde or ketone and isoxazolyamines as starting materials (Scheme 2). To the proper isoxazolyamine (10.2 mmol), dissolved acetic acid/dichloroethane (1:5 v/v, 20 ml), aldehyde or ketone was added (20.4 mmol). The solution thus obtained was warmed at 60 °C for 1.5 h, under magnetic stirring. Sodium triacetoxyborohydride (18.4 mmol) was then added portionwise, and the reaction was maintained at the same temperature. After 3.5 h the mixture was cooled and NaOH 1 N (15 ml) was added. The organic phase was separated and extracted one more time with the alkaline solution. Then it was dried over Na_2SO_4 , filtered and concentrated *in vacuo*. The crude products were purified by column chromatography using mixtures of *n*-hexane/ethyl acetate as eluent. Final products were crystallized, if



Scheme 2. Representation of the synthesis procedure for all isoxazolyamine derivatives of the present study (see [Experimental section](#) for details) and classification of the substituent groups present in each compound.

Compound	X	Y	R1	R2	R3
1a	O	N	CH ₃	CH ₃	CH ₃
1b	O	N	CH ₃	(CH ₃) ₂ CH	H
1c	O	N	CH ₃	(CH ₃) ₂ CHCH ₂	H
1d	O	N	CH ₃	CH ₃ CH ₂ CH ₂	H
1e	O	N	CH ₃		H
1f	O	N	CH ₃		H
1g	O	N	CH ₃		H
1h	O	N	CH ₃		H
2b	N	O	CH ₃	(CH ₃) ₂ CH	CH ₃
2d	N	O	CH ₃	CH ₃ CH ₂ CH ₂	H
3b	O	N	H	(CH ₃) ₂ CH	CH ₃
3d	O	N	H	CH ₃ CH ₂ CH ₂	H

possible, by mixtures of *n*-hexane/ethyl acetate and were easily obtained in excellent yields (62–73%).

2.2. Characterization of TRPM8-mediated menthol-induced $[Ca^{2+}]_i$ increase in F11 cells

F11 cells, a cloned cell line obtained by the fusion of embryonic rat dorsal root ganglion (DRG) neurons with mouse neuroblastoma cells [24], have been widely used to study nociceptive molecular mechanisms [25]. RT-PCR experiments revealed the expression of TRPM8 transcripts in undifferentiated F11 cells (expected size of the band: about 130 bp; insert in [Fig. 1A](#)). Furthermore, quantitative real time PCR revealed that differentiated F11 cells showed a 4-fold increase in TRPM8 transcript expression when compared to undifferentiated cells ([Fig. 1A](#)). Based on these results, following experiments were performed in differentiated cells. As previously demonstrated in TRPM8-expressing cells [6], exposure of F11 cells to *L*-menthol (3–300 μ M) for 20 s led to a transient, concentration-dependent increase in intracellular Ca^{2+} concentrations $[Ca^{2+}]_i$ ([Fig. 1B](#)). The calculated EC_{50} for menthol-induced $[Ca^{2+}]_i$ increase was 23.4 ± 2.6 μ M ([Fig. 1C](#)), a value consistent with previous reports [26,27]. Menthol-induced $[Ca^{2+}]_i$ response displayed a very rapid onset (within about 1 s), and peaked after 10–15 s. By contrast, the kinetics of $[Ca^{2+}]_i$ decline following menthol removal from the bath appeared to depend on agonist concentration, being slower at higher menthol concentrations (range between 50 and 400 s). The effect of menthol (100 μ M) on $[Ca^{2+}]_i$ levels in F11 cells was fully prevented by the TRPM8 antagonist BCTC (3 μ M) [28] ([Fig. 1D](#)) or by agonist exposure in a Ca^{2+} -free solution (plus 1 mM EDTA) ([Fig. 1D](#)). These observations suggest that menthol-induced enhancement of $[Ca^{2+}]_i$ was due to its ability to activate TRPM8 channels, and depended on an enhanced flux of extracellular Ca^{2+} ions across the plasma membrane.

2.3. Pharmacological properties of newly synthesized aminoisoxazole derivatives

In the present study, 12 new isoxazole derivatives were synthesized, bearing substituents at position 3 and 5 of the heteroaromatic ring (see [Scheme 2](#)), to define the best structural requirements for the pharmacological activity of each compound. In particular aminoaliphatic (**1a–e**) and aminoaromatic (**1f–h**) chains were introduced at position 3 for derivatives belonging to series **1**, while a methyl group occupies position 5. By contrast,

derivatives belonging to the series **3** (**3b** and **3d**) lack the methyl group in position 5. Finally, the derivatives **2b** and **2d** are isomers of **1b** and **1d**, due to inversion of the oxygen and nitrogen heteroatoms.

To characterize their pharmacological activity as TRPM8 agonists *in vitro*, these new compounds were tested for their ability to enhance $[Ca^{2+}]_i$ in differentiated F11 cells, as previously shown for menthol. All tested molecules increased $[Ca^{2+}]_i$ in a concentration-dependent manner, although with different efficacy and potency ([Fig. 2A–N](#)). To simplify comparison of the efficacy among tested compounds, the maximal fluorescent increase prompted by each compound was normalized to the maximal response produced by menthol. As reported in [Table 1](#), none of the tested compounds showed a higher efficacy than menthol. The compounds referred as **1d** and **1f** showed the same efficacy than menthol ($p > 0.05$); instead, the other ten tested compounds were less effective than menthol, showing the following rank order of efficacy: **1g** > **3b** > **3d** > **1h** > **1c** > **1e** > **1b** > **1a** > **2b** > **2d**, suggesting that longer aliphatic chains or aromatic substituents at the position R2 are required to retain high efficacy.

By contrast, comparison of the potency among tested compounds was performed by normalization of the experimental data to the maximal value of fluorescence ratio prompted by each compound. As shown in [Fig. 3](#) and summarized in [Table 1](#), eight of the tested compounds (i.e. **1a–e**, **1h**, **3b**, **3d**) showed a significantly lower EC_{50} when compared to menthol, suggesting that aliphatic substituents at the R2 and R1 positions are involved in conferring high potency to the tested compounds. The compound referred as **1g** showed the same potency as menthol ($p > 0.05$); finally, the other three tested compounds were less potent than menthol, with the following rank order of potency: **2b** > **2d** > **1f**, suggesting that the introduction of an aromatic ring at the position R2 or the inversion of the heteroatoms at the position X, Y (see [Scheme 2](#)) have deleterious effects on compound potency.

As later detailed in the [Discussion](#) paragraph, the reported newly-synthesized molecules can be roughly subdivided into two groups: the first includes compounds characterized by sub-micromolar potency but with quite low efficacy (as seen for example in **1a–c** derivatives), and the second includes compounds endowed with low potency and high efficacy (as exemplified by **1f** and **1g**). The compound **1d** appears to be the most promising compromise since it shows low micromolar potency combined with a very remarkable efficacy.

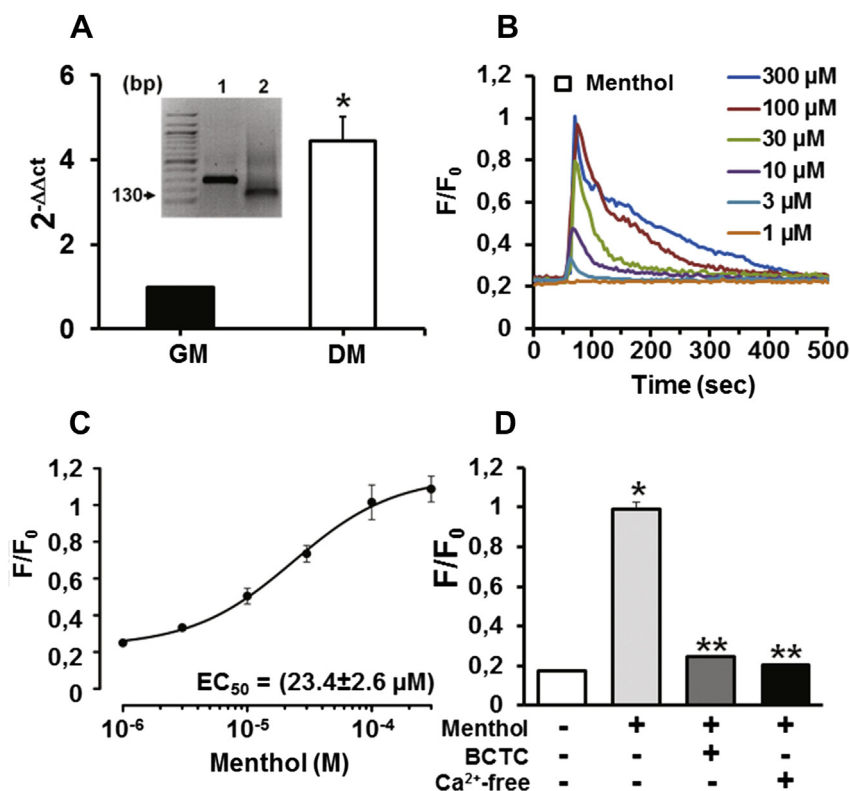


Fig. 1. Expression of TRPM8 transcripts in F11 cells and characterization of the menthol-induced responses. (A) The insert indicates the RT-PCR obtained by mRNA from undifferentiated F11 cells. The amplicon expected size for TRPM8 was 130 bp (lane 2), as indicated. GAPDH was used as housekeeping gene (amplicon expected size: 300 bp, lane 1). Quantitative real-time PCR on the total mRNA of undifferentiated (GM; black bar) or differentiated (DM; white bar) F11 cells. Data are expressed as $2^{-\Delta\Delta ct}$ relative to GAPDH (see Experimental section for details). Each bar is the mean \pm S.E.M. of three separate determinations; * $p < 0.05$ versus control (F11 cells in GM). (B) Representative traces of the changes in fluorescence ratio (F/F_0) evoked by 1 μ M (orange trace), 3 μ M (sky-blue), 10 μ M (violet), 30 μ M (green), 100 μ M (brown), or 300 μ M (blue) menthol. The bar length on the top of all traces corresponds to the duration of drug exposure. (C) Concentration–response curve from the experimental data obtained as in C. The solid line represents the fit of the experimental data to a standard binding equation of the following form: $y = \max/(1 + x/EC_{50})^n$, where x is the drug concentration and n the Hill coefficient; n was 1.1 ± 0.1 . Each point is the mean \pm S.E.M. of 23–28 separate determinations performed in at least 3 experimental sessions. (D) Quantification of the fluorescence ratio (F/F_0) peaks measured in differentiated F11 cells at basal levels or after the exposure to 100 μ M menthol in a control solution, in co-perfusion with the TRPM8 antagonist BCTC (3 μ M) or in a Ca^{2+} -free solution. Each bar represents the average of 12–23 determinations obtained in at least 3 experimental sessions.

2.4. Pharmacological effects of selected aminoisoxazole derivatives on acetone-induced allodynic responses in rat with chronic constriction injury (CCI) of the sciatic nerve

Based on the *in vitro* results, we compared the effects of the most potent compounds (**1a–d**) with those of menthol in the CCI rat model of cold allodynia. To this aim, 50 μ l of each compound (dissolved in 20% w/v in absolute ethanol) were topically (transdermally) applied on the operated paw, and the allodynic responses (number of paw retraction) to three consecutive application of acetone (each lasting 2 min, applied every 7 min, see protocol in Fig. 4A) were evaluated 14 days after sciatic nerve ligation. When the total number of allodynic responses occurring during acetone application were measured, it was observed that local application of menthol, **1a**, **1b**, or **1c** elicited similar cold allodynic responses, whereas **1d** and **1f** were ineffective ($p > 0.05$ versus vehicle; Fig. 4B). However, when the effects of the TRPM8 activators were measured after each of the three consecutive acetone applications, it was found that menthol failed to produce a significant effect of cold allodynia after the first (Fig. 4C) and the third (Fig. 4E) acetone application, while significant effects were detected after the second acetone exposure (Fig. 4D). By contrast, the time-dependence of the allodynic responses triggered by the newly synthesized compounds was clearly distinct from that of menthol, showing faster onset and offset kinetics. In fact, compounds **1a–d** were efficacious after the first acetone application (Fig. 4C), whereas they failed to

induce cold allodynia after the second and third challenge (Fig. 4D and E). At least for **1a–c**, allodynic responses were stronger than those observed with menthol after any acetone challenge. Instead, **1f**, the compound showing the lowest potency in *in vitro* testing, did not produce cold allodynia after any acetone application (Fig. 4C–E).

2.5. Computational studies

To identify the structural elements involved in the interactions of the here reported isoxazole derivatives with the TRPM8 channel which might provide a plausible explanation for their different pharmacological properties, docking simulations of these molecules on the recently reported structural model of the human TRPM8 receptor [23] were performed. As shown in Fig. 5A, the main interactions stabilizing the complex between TRPM8 and the most potent **1a** derivative occur in a subpocket adjacent, but not coincident, with that of menthol, roughly corresponding to that occupied by the nitrophenyl moiety of icilin [23].

This result emphasizes the role of N799, which stabilizes an extended π – π stacking involving the carbamido function of the aminoacid side chain and the entire isoxazole ring. Furthermore, ligand's amino group is involved in an H-bond with the D802 carboxylate, a further key residue determining the activity of icilin, as also demonstrated by mutagenesis [26]. Finally, the interaction between ligand and the D802 seems to be essential for agonism as

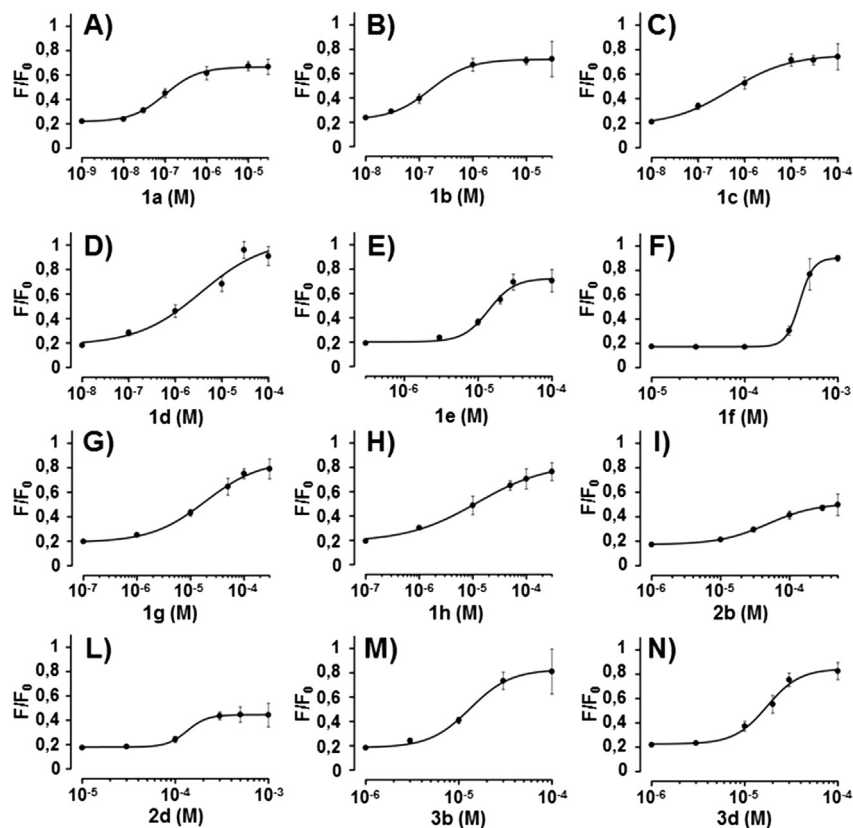


Fig. 2. Concentration-dependent effects of isoxazole derivatives. (A–N) Concentration–response curves in terms of Fura-2 fluorescence ratio (F/F_0) obtained upon perfusion of **1a** (0.001–30 μ M), **1b** (0.01–30 μ M), **1c** (0.01–100 μ M), **1d** (0.01–100 μ M), **1e** (0.3–100 μ M), **1f** (10–1000 μ M), **1g** (0.1–300 μ M), **1h** (0.1–300 μ M), **2b** (1–500 μ M), **2d** (10–1000 μ M), **3b** (1–100 μ M), **3d** (1–100 μ M) compounds on differentiated F11 cells. The solid lines represent the fit of the experimental data to a standard binding equation (see above). Each point is the mean \pm S.E.M. of 27–63 separate determinations performed in at least 3 experimental sessions. The effects of all compounds are represented on the same Y scale to facilitate comparison.

it destroys the H-bond between D802 and Y745, which characterizes the inactive state of TRPM8 channels, thus triggering its activation [29]. These two major contacts are further stabilized by a set of hydrophobic interactions with surrounding apolar side chains (e.g. L749, A753 and F794).

Notably, the isopropyl group of the **1a** derivative approaches Y745 contacting the apolar residues involved in the interactions with menthol, while the ligand's methyl group seems to act as a

pivot which restrains the ligand pose within the binding site, thus maximizing its interactions (see below). Accordingly, docking results show that the desmethyl analogue (**3b**) is characterized by a slightly different pose, in which the ligand slides towards F794 and loses its key H-bond with D802. Again, the isopropyl chain affords the best potency presumably because it balances apolar contacts and steric hindrance, while bulkier groups (such as in **1b** or in **1d**) tend to clash against Y745 or L749. Interestingly, the isopropyl

Table 1
Pharmacological properties of isoxazole derivatives.

Compound	Potency EC ₅₀ (μ M)	Efficacy (% Menthol maximal response)
Menthol	23.4 \pm 2.6	100%
1a	0.10 \pm 0.01 ^{##}	53 \pm 4%*
1b	0.16 \pm 0.01 ^{##}	58 \pm 4%*
1c	0.5 \pm 0.1 ^{##}	66 \pm 4%*
1d	3.6 \pm 3.5 ^{##}	89 \pm 8%
1e	13.9 \pm 1.5 [#]	64 \pm 7%*
1f	400.0 \pm 1.4 [†]	82 \pm 9%
1g	18.9 \pm 3.6	74 \pm 5%*
1h	12.0 \pm 2.9 [#]	66 \pm 6%*
2b	48.4 \pm 3.7 [†]	36 \pm 4%**
2d	100.0 \pm 5.6 [†]	32 \pm 3%**
3b	13.2 \pm 1.3 [#]	72 \pm 8%*
3d	17.3 \pm 1.6 [#]	69 \pm 6%*

[#]Potency values significantly ($p < 0.05$) lower than menthol.

^{##}Potency values significantly ($p < 0.05$) lower than compound with #.

[†]Potency values significantly ($p < 0.05$) higher than menthol.

*Efficacy values significantly ($p < 0.05$) lower than menthol.

**Efficacy values significantly ($p < 0.05$) lower than compound with *.

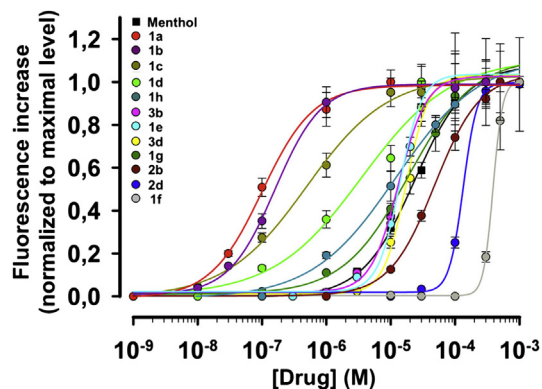


Fig. 3. Concentration–response curves for all newly synthesized isoxazole derivatives. F/F_0 fluorescent ratios obtained from Fig. 2A–N were divided by the maximal fluorescent increase obtained for each compound and subtracted by the fluorescent ratio at the lowest drug concentration. The solid lines represent the fit of the normalized data to a standard binding equation (see above) and are indicated in different colors for each compound, as indicated.

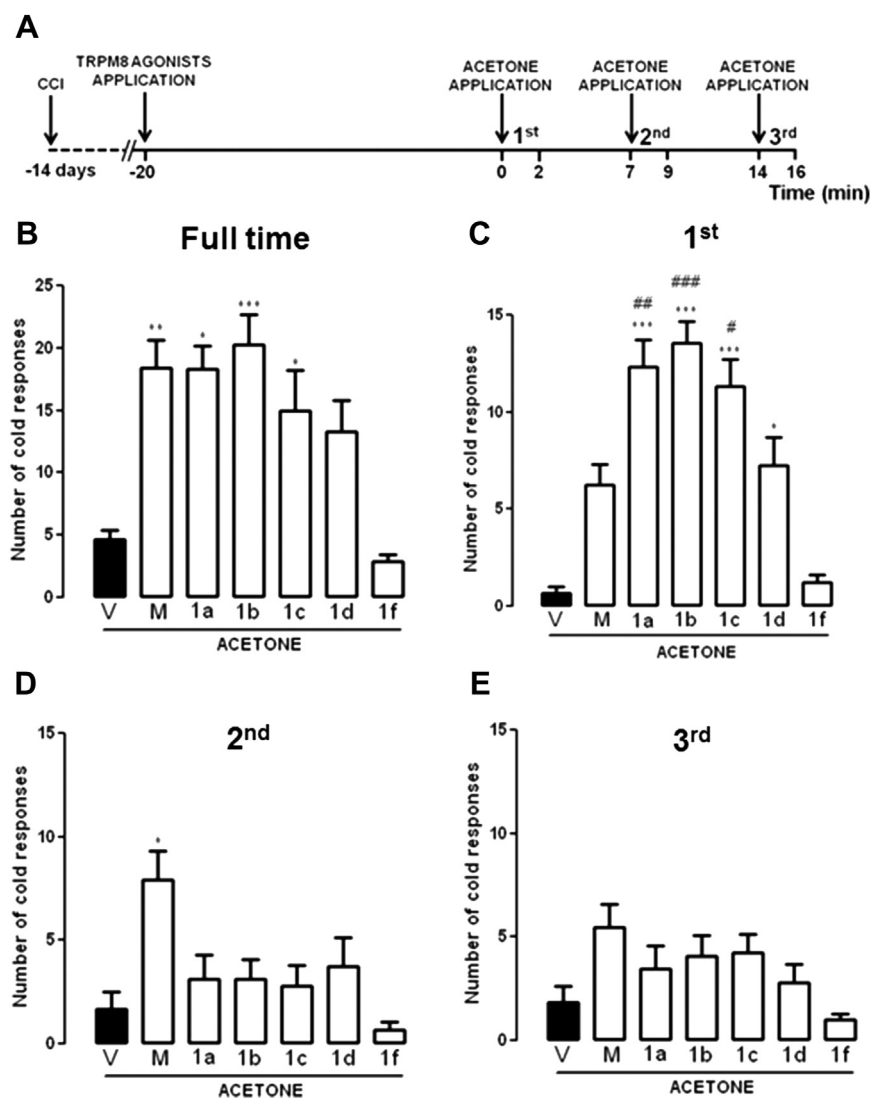


Fig. 4. Quantification of the cold responses evoked by the newly-synthesized compounds *in vivo*. (A) Schematization of the time procedure followed for the experiments plotted in B, C, D and E. (B) Total number of the cold responses measured during the full-time experiment after 20 min of preincubation with the indicated compounds in CCI mice treated with acetone. (C, D, E) Time-course of the cold responses prompted upon topical application of vehicle (V), menthol (M) or the indicated compounds on the effects evoked by acetone on CCI mice during the first (C), second (D) or the third (E) phase of the experiment. Data are the mean \pm SEM ($n = 6$). * $p < 0.05$, ** $p < 0.01$, *** $p < 0.001$, all versus vehicle; $p < 0.05$, $p < 0.01$, $p < 0.001$, all versus menthol.

group corresponds to the substituent also inserted in a comparable pose by menthol, suggesting that this group best fits the TRPM8 cavity in that region.

By contrast, when the N-linked group is further enlarged, as seen in the **1f–h** derivatives, the resulting ligands cannot assume the above described pose and show a completely different arrangement in which the isoxazole ring approaches Y745, while the bulky N-linked moiety approaches N799. Fig. 5B displays the pose of the **1h** derivative showing that the isoxazole ring is unable to elicit both significant π – π stacking and the key H-bond with Y745. The nitrophenyl moiety mimics the pose assumed by the same group of icilin stabilizing a key H-bond which involves the nitro function and the side chain of N799, while the amino group of **1h** interacts with D802. However, the inability to contact Y745 as well as the steric clashes exerted with surrounding residues could explain its poor potency, an effect which appears to be dramatically exacerbated when the ligand cannot elicit H-bonds with N799 (as seen for **1f**). Finally, docking simulations revealed that the inverted 3-methyl derivatives (**2b** and **2d**) assume a different pose which

could explain their poor potency. In detail, their isoxazole ring stabilizes an H-bond between the intra-annular oxygen atom and the N799 side chain, losing the extended π – π stacking and, more importantly, these compounds appear to be unable to elicit the pivotal contact with D802.

3. Conclusion

In the present study, the pharmacological properties of newly synthesized aminoisoxazole derivatives with respect to their ability to act as novel TRPM8 agonists have been studied using $[Ca^{2+}]_i$ -imaging experiments in sensory neurons *in vitro*, and an *in vivo* model of cold allodynia. The use of an isoxazole ring as key scaffold for these molecules was chosen because of many chemical considerations (see below); modifications on this scaffold mainly concerned the introduction of a secondary amine group linked to different aliphatic chains in the position 3 of the isoxazole ring and/or the introduction of a methyl group in the position 5.

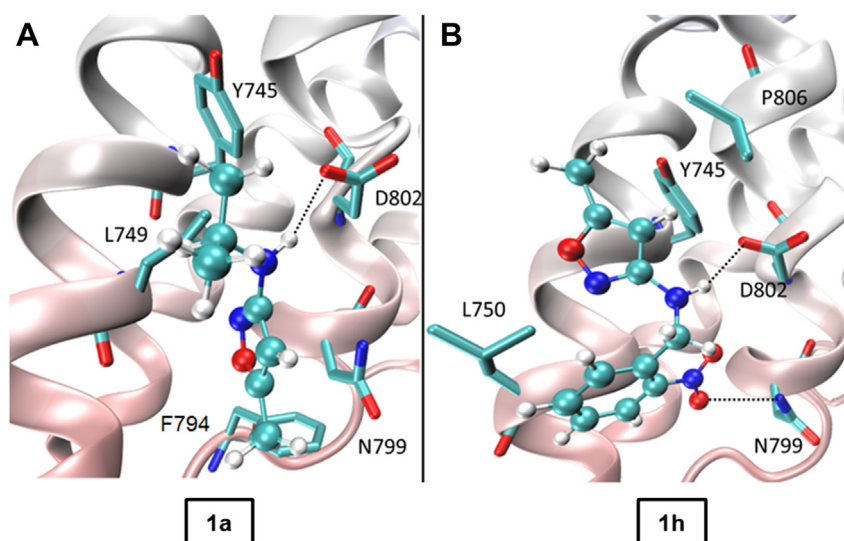


Fig. 5. Magnification of the binding site in TRPM8 channel. (A, B) Main interactions stabilizing the complex between the TRPM8 binding site and **1a** (A) or **1h** (B). The cartoon for the transmembrane helices is colored according to their orientation within the membrane bilayer (gray = extracellular side; pink = intracellular side).

When tested *in vitro*, the compounds containing modifications only at the 3-position, particularly a secondary amine linked to an isobutyl (**3b**) or a butyl (**3d**) group, displayed a slightly higher potency when compared to menthol, whereas their efficacy was slightly reduced. The introduction of a methyl group at the 5-position in both these compounds (generating **1b** and **1d**, respectively), lead to a further improvement of the potency, without altering the efficacy in the case of **1b** or inducing a small, but significant efficacy increase in the case of **1d** when compared to **3d**. Further modifications of the aliphatic chain connected with the secondary amine (consisting in an isopropyl or an isobutyl group in the case of **1a** or **1c**, respectively) prompted to similar improvement in the potency, but still not in the efficacy, when compared to the parent compounds (**3b** or **3d**).

The increase in potency showed by the described compounds is instead prevented by the introduction of an aromatic function on the groups linked to the amine at the 3-position of the isoxazole ring. In fact, when a benzyl group was linked to the secondary amine (**1f**), a dramatic decrease in potency was observed; furthermore, when this high electron density group was depleted through the introduction of the known deactivator $-\text{NO}_2$ (at the *ortho*- or *para*-position, as in the **1h** and **1g** derivatives, respectively) or replaced by a cyclohexyl group (**1e**), the potency increased by about 20-fold.

To test *in vivo* the effects of the compounds showing the highest TRPM8-activating potencies *in vitro* (**1a**, **1b**, **1c** or **1d**), we used the acetone-induced cold allodynia model in CCI mice [30,31]. In this test, evaporative cooling of locally applied acetone is used to evoke nociceptive behavior; pharmacological [32] and genetic [14] evidence suggest that the activation of TRPM8 channels plays a central role in this *in vivo* model. Moreover, in addition to acetone, menthol can trigger TRPM8-dependent allodynic responses in mice with CCI [33]. In accordance with this, we observed that, similarly to menthol, the newly-synthesized **1a–d** compounds, also potentiated allodynic responses prompted by acetone exposure, suggesting that they also acted as TRPM8 agonists. However, when compared to menthol, **1a–d** showed a distinct time-dependent profile. In fact, allodynic responses triggered by these compounds showed a shorter latency, being already evident after the first triggering stimulus was applied; in addition, **1a–1d** compounds ceased to elicit allodynic responses after the second or third acetone application. By contrast, menthol was only effective after

the second acetone application, and the **1f** compound failed to display allodynic effects at any time point after stimulus challenge. These observation suggests the existence of a good correspondence between *in vitro* and *in vivo* data, with those compounds showing the highest *in vitro* potency as TRPM8 agonists being provided of faster onset and offset *in vivo* effects when compared to menthol, and the lower potency TRPM8 agonist showing no efficacy in *in vivo* testing. As mentioned in the Results paragraph, the *in vitro* pharmacological profile shown by the newly-synthesized molecules allows to classify them in menthol-like derivatives, characterized by high efficacy but quite low potency, and icilin-like derivatives, the latter showing remarkable submicromolar potencies but characterized by an efficacy lower than that of menthol. The results achieved in our docking experiments suggest valid structural hypothesis to rationalize these biological evidence. Indeed, the computed complexes suggest that the TRPM8 binding site can be roughly subdivided into two regions. The first region is more hydrophobic, and contains the Y745 residue playing a key role in TRPM8 activation [34]. Given the nature of the flanking residues, a ligand can occupy such a region by stabilizing a set of precise hydrophobic contacts plus key H-bonds with Y745, as seen for the prototypical example of menthol. The second region is more polar as it is lined by N799 and D802 which can elicit reinforced H-bonds and extended π - π stacking with the more potent isoxazole derivatives. When considering these possible polar interactions, it comes as no surprise that suitable ligands which occupy this second region can afford markedly higher potencies compared to ligands which are positioned in the first subcavity where at most they stabilize H-bonds with Y745. Yet, the ability of molecules to interact with residues of the first region appears to be an essential requisite to achieve a good efficacy profile, regardless of the polar contacts stabilized within the second subpocket. Notably, icilin confirms that ligands able to suitably occupy both subpockets can successfully combine potency and efficacy even though such a double occupation appears to be vastly constrained by hampering steric clashes exerted by surrounding apolar residues.

Taken together, the results obtained emphasize that the newly synthesized compounds (particularly **1a–c**) can induce TRPM8 activation *in vivo*. Although the TRPM8-dependent acetone test in CCI animals utilized in our study is a model of cold allodynia (indicative of an increased pain sensitivity), it should be reminded that the activation of TRPM8 channels can also mediate analgesic

effects [35]. As a matter of fact, menthol itself, though acting as a reference compound for TRPM8 activators, has well-known analgesic properties [36]. Concentration-dependent effects of menthol at TRPM8 receptors might provide a plausible explanation for this apparently paradoxical behavior; in fact, while, as indicated previously, elevated concentration of menthol trigger TRPM8-dependent nociceptive behavior in CCI mice [14,33], lower menthol concentrations induced marked analgesia in the same rat model of neuropathic pain [9]. However, whether additional variables such as changes in TRPM8 kinetics of activation and/or desensitization, differential treatment modalities (topical vs systemic administration), or model-dependent effects on TRPM8 expression levels at various sites contribute to the distinct pharmacological profile shown *in vivo* by menthol or other TRPM8 modulators remains to be investigated.

Despite all these uncertainties, the present results clearly suggest that presently-described aminoisoxazole-based derivatives display a pharmacological profile, both *in vitro* and *in vivo*, consistent with that of TRPM8 agonists. Thus, we believe that these molecules might be of considerable interest for further structural optimization and functional analysis, in order to validate their clinical utility as novel analgesics.

4. Experimental protocols

4.1. General

L-Menthol, as well all other chemicals and solvents were furnished by Sigma–Aldrich (Milan, Italy). Course of reactions and purity of finished product was estimated by TLC, using precoated silica gel glass plates (Macherey Nagel, Duren, Germany). Preparative separations were performed in glass columns packed with silica gel (Macherey Nagel; Ø 0.063:0.200 mm). All other solvents and reagents were of analytical grade. Melting points were determined using a Büchi apparatus B 540 and are uncorrected. ^1H NMR and ^{13}C NMR were recorded using a Varian Mercury 400 instrument (Varian inc., Palo Alto, USA). Chemical shifts are reported in δ units (ppm) relative to tetramethylsilane used as internal standard. The following symbols were used to describe the NMR peaks: s = singlet, bs = broad singlet, d = doublet, dd = double doublet, pd = pseudo-doublet, t = triplet, pt = pseudo-triplet, m = multiplet. Mass spectra were recorded using an API 2000 spectrometer (Applied Biosystem, Monza, Italy). Elemental analysis was carried on using a 2400 Perkin–Elmer CHN Analyzer (Perkin Elmer Italia, Monza, Italy). Results obtained were within $\pm 0.4\%$ of theoretical values. Derivatives belonging to series 1 were synthesized starting from 3-amino-5-methyl isoxazole, while derivatives belonging to series 2 and 3 were synthesized from 5-amino-3-methyl isoxazole and 3-aminoisoxazole respectively.

4.2. General procedure for the synthesis of isoxazolyamine derivatives

4.2.1. *N*-(Methyl)ethyl-*N*-(5-methyl-3-isoxazolyl)amine (**1a**)

Compound **1a** was obtained starting from acetone. Crude product was purified using *n*-hexane/ethyl acetate (9/1) as eluent. Final product was crystallized from *n*-hexane as a white solid (1.0 g, yield 73%). M.p. = 93–95 °C. ^1H NMR (CDCl_3): δ 5.49 (s, 1H), 3.73–3.63 (m, 1H, $J = 25.0$ Hz), 3.25 (bs, 1H, D_2O exchangeable), 2.30 (s, 3H), 1.23 (d, 6H, $J = 6.2$ Hz); ^{13}C NMR (CDCl_3): δ 168.4, 164.4, 93.2, 45.5, 23.1, 12.5. MS (m/z): 140.95 (M + H) $^+$.

4.2.2. *N*-(2-Methyl)propyl-*N*-(5-methyl-3-isoxazolyl)amine (**1b**)

The product was synthesized starting from 2-methylpropanal. Crude product was purified using *n*-hexane/ethyl acetate (9/1) as

mobile phase. Final product was crystallized from *n*-hexane as a white solid (1.0 g, yield 67%). M.p. = 97–99 °C; ^1H NMR (CDCl_3): δ 5.51 (s, 1H), 3.85 (bs, 1H, D_2O exchangeable), 3.00 (t, 2H, $J = 13.0$ Hz), 2.31 (s, 3H), 1.95–1.85 (m, 1H, $J = 25.7$ Hz), 0.97 (d, 6H, $J = 6.6$ Hz); ^{13}C NMR (CDCl_3): δ 168.5, 164.6, 92.9, 48.4, 26.7, 20.9, 12.4. MS (m/z): 155.61 (M + H) $^+$.

4.2.3. *N*-(3-Methyl)butyl-*N*-(5-methyl-3-isoxazolyl)amine (**1c**)

The product was synthesized starting from 3-methylbutanal. Crude product was purified using *n*-hexane/ethyl acetate (9.5/0.5) as mobile phase and was isolated as a white solid after crystallization from hexane (1.18 g, yield 69%). M.p. = 87–89 °C. ^1H NMR (CDCl_3): δ 5.52 (s, 1H), 3.68 (bs, 1H, D_2O exchangeable), 3.25–3.19 (m, 2H, $J = 15.0$ Hz), 2.30 (s, 3H), 1.62–1.58 (m, 1H, $J = 19.6$ Hz), 1.50–1.45 (m, 2H, $J = 22.4$ Hz), 0.95 (d, 6H, $J = 6.8$ Hz); ^{13}C NMR (CDCl_3): δ 168.7, 166.1, 92.4, 48.2, 36.6, 26.2, 22.8, 12.9. MS (m/z): 155.73 (M + H) $^+$.

4.2.4. *N*-Butyl-*N*-(5-methyl-3-isoxazolyl)amine (**1d**)

The product was synthesized starting from *n*-butanal. Crude product was purified using *n*-hexane/ethyl acetate (9/1) as mobile phase. Final product was isolated as a colorless oil that did not crystallize (0.95 g yield 62%). ^1H NMR (CDCl_3): δ 5.50 (s, 1H), 3.74 (bs, 1H, D_2O exchangeable), 3.21–3.18 (m, 2H, $J = 20.1$ Hz), 2.28 (s, 3H), 1.63–1.53 (m, 2H, $J = 30.5$ Hz), 1.37–1.29 (m, 2H, $J = 37.4$ Hz), 0.96 (t, 3H, $J = 14.7$ Hz); ^{13}C NMR (CDCl_3): δ 168.8, 165.3, 92.8, 44.0, 32.1, 22.0, 14.0, 12.7. MS (m/z): 169.91 (M + H) $^+$.

4.2.5. *N*-Cyclohexylmethyl-*N*-(5-methyl-3-isoxazolyl)amine (**1e**)

The product was synthesized starting from cyclohexanecarbaldehyde. Crude product was purified using *n*-hexane/ethyl acetate (9.8/0.2) as mobile phase. Final product was obtained as colorless oil (1.36 g, yield 70%). ^1H NMR (CDCl_3): δ 5.50 (s, 1H), 3.99 (bs, 1H, D_2O exchangeable), 3.05 (t, 2H, $J = 13.4$ Hz), 2.27 (s, 3H), 1.75–1.65 (m, 5H), 1.26–1.12 (m, 4H, $J = 54$ Hz), 0.93–0.84 (m, 2H, $J = 34$ Hz); ^{13}C NMR (CDCl_3): δ 168.3, 166.5, 92.7, 57.6, 36.6, 31.1, 26.7, 26.0, 12.8. MS (m/z): 195.95 (M + H) $^+$.

4.2.6. *N*-Benzyl-*N*-(5-methyl-3-isoxazolyl)amine (**1f**)

The product was synthesized starting from benzaldehyde. Crude product was purified using *n*-hexane/ethyl acetate (9/1) as mobile phase. Final product was obtained as a pale yellow solid after crystallization in diethyl ether (1.39 g, yield 73%). Spectral data and melting point were in accordance with literature [37]. MS (m/z): 189.40 (M + H) $^+$.

4.2.7. *N*-(4'-Nitro)benzyl-*N*-(5-methyl-3-isoxazolyl)amine (**1g**)

The product was synthesized starting from 4-nitrobenzaldehyde. Crude product was purified using *n*-hexane/ethyl acetate (7/3) as mobile phase. Final product was obtained as a yellowish solid after crystallization in diethyl ether (1.62 g, yield 69%). M.p. = 108–109 °C. ^1H NMR (CDCl_3): δ 8.22 (pd, 2H, $J = 8.3$ Hz), 7.56 (pd, 2H, $J = 8.1$ Hz), 5.53 (s, 1H), 4.55 (d, 2H, $J = 6.0$ Hz), 4.32 (bs, 1H, D_2O exchangeable), 2.32 (s, 3H); ^{13}C NMR (CDCl_3): δ 169.5, 164.4, 147.4, 146.8, 128.2, 124.1, 93.2, 47.5, 12.8. MS (m/z): 234.72 (M + H) $^+$.

4.2.8. *N*-(2'-Nitro)benzyl-*N*-(5-methyl-3-isoxazolyl)amine (**1h**)

The product was synthesized starting from 2-nitrobenzaldehyde. Crude product was purified using *n*-hexane/ethyl acetate (7/3) as mobile phase. Final product was obtained as a gray solid after crystallization in diethyl ether (1.5 g, yield 63%). M.p. = 98–99 °C. ^1H NMR (CDCl_3): δ 8.10 (pd, 1H, $J = 8.1$ Hz), 7.77 (pd, 1H, $J = 7.3$ Hz), 7.64 (pt, 2H, $J = 15.0$ Hz), 7.47 (pt, 2H, $J = 14.8$ Hz), 5.51 (s, 1H), 4.73 (d, 2H, $J = 6.6$ Hz), 4.65 (bs, 1H, D_2O exchangeable), 2.30 (s, 3H); ^{13}C NMR (CDCl_3): δ 169.2, 164.4, 148.5, 134.7, 134.1, 132.0, 128.7, 125.4, 93.5, 45.7, 12.7. MS (m/z): 235.01 (M + H) $^+$.

4.2.9. *N*-(2-Methyl)propyl-*N*-(3-methyl-5-isoxazolyl)amine (**2b**)

Derivative **2b** was synthesized as previously described for **1b**. Final product was crystallized from petroleum ether as a gray solid (1.1 g yield 72%). M.p. = 110–112 °C. ¹H NMR (CDCl₃): δ 4.82 (s, 1H), 4.62 (bs, 1H, D₂O exchangeable), 2.97 (t, 2H, *J* = 13.0 Hz), 2.17 (s, 3H), 1.91–1.86 (m, 1H, *J* = 25.8), 0.97 (d, 6H, *J* = 6.5 Hz); ¹³C NMR (CDCl₃): δ 170.3, 161.6, 77.8, 52.4, 28.5, 20.2, 12.0. MS (*m/z*): 155.41 (M + H)⁺.

4.2.10. *N*-(Butyl)-*N*-(3-methyl-5-isoxazolyl)amine (**2d**)

The product was synthesized according to the procedure adopted for **1d**. Final Product was crystallized from petroleum ether as a gray solid (1.0 g) yield 64%. M.p. = 84–86 °C. ¹H NMR (CDCl₃): δ 4.85 (s, 1H), 4.62 (bs, 1H, D₂O exchangeable), 3.17–3.14 (m, 2H, *J* = 19.9 Hz), 2.19 (s, 3H), 1.52–1.41 (m, 2H, *J* = 30.8 Hz), 1.38–1.32 (m, 2H, *J* = 37.5 Hz), 0.95 (t, 3H, *J* = 14.7 Hz); ¹³C NMR (CDCl₃): δ 170.1, 162.8, 77.9, 43.2, 31.3, 19.9, 13.4, 12.1. MS (*m/z*): 170.01 (M + H)⁺.

4.2.11. *N*-(2-Methyl)propyl-*N*-(3-isoxazolyl)amine (**3b**)

The product was synthesized according to the procedure adopted for **1b**. Purification was carried out using *n*-hexane/ethyl acetate (6/4) as mobile phase. Final product was crystallized from hexane and was isolated as a white solid (1.1 g yield 74%). M.p. = 46–48 °C; ¹H NMR (CDCl₃): δ 8.00 (pd, 1H, *J* = 1.6 Hz), 5.84 (pd, 1H, *J* = 1.6 Hz), 3.94 (bs, 1H, D₂O exchangeable), 3.05 (t, 2H, *J* = 13.1 Hz), 1.93–1.85 (m, 1H, *J* = 25.4 Hz), 0.95 (d, 6H, *J* = 6.6 Hz); ¹³C NMR (CDCl₃): δ 164.2, 157.8, 95.8, 51.9, 28.4, 20.1. MS (*m/z*): 141.55 (M + H)⁺.

4.2.12. *N*-Butyl-*N*-(3-isoxazolyl)amine (**3d**)

The product was synthesized according to the procedure adopted for **1d**. Mobile phase consisted in *n*-hexane/ethyl acetate (8/2). Final product was isolated as pale yellow oil (1.0 g, yield 70%). ¹H NMR (CDCl₃): δ 8.07 (pd, 1H, *J* = 1.5), 5.83 (pd, 1H, *J* = 1.5), 3.90 (bs, 1H, D₂O exchangeable), 3.25–3.21 (m, 2H, *J* = 20.0 Hz), 1.69–1.58 (m, 2H, *J* = 30.7 Hz), 1.47–1.39 (m, 2H, *J* = 37.6), 0.96 (t, 3H, *J* = 14.7 Hz); ¹³C NMR (CDCl₃): δ 164.2, 157.7, 96.0, 43.8, 31.0, 19.9, 13.7. MS (*m/z*): 142.41 (M + H)⁺.

4.3. Pharmacology

4.3.1. Cell cultures

F11 cells were grown and differentiated as recently reported [38]. Briefly, these cells were grown in DMEM medium supplemented with 10% FBS, 1% penicillin/streptomycin (10 U/μl) and 1% L-glutamine (200 mM) (referred as GM). The cells were kept in a humidified atmosphere at 37 °C with 5% CO₂ in 100-mm plastic Petri dishes F11 cell differentiation was achieved upon at least 72 h cell exposure to a differentiation medium (referred as DM) containing a lower FBS concentration (2%) and 10 μM retinoic acid. For calcium-imaging experiments, F11 cells were plated on glass coverslips (Carolina Biological Supply Co., Burlington, NC) coated with poly-L-lysine (SIGMA, Milan, Italy); 24 h after plating, F11 cells were exposed to the DM.

4.3.2. PCR analyses

Total RNA from undifferentiated or differentiated F11 cells using TRI-Reagent (Sigma–Aldrich, Milan, Italy) was treated with DNase 1 U/μl for 15 min at room temperature and quantified by spectrophotometry (260 nm/280 nm ratio >1.7). Thereafter, 5 μg of the isolated RNA was used as template for the synthesis of cDNA by reverse transcription at 37 °C for 2 h. PCR reactions were carried out on an AmpliTaq Gold 0.25 U/μl (Applied Biosystem, Monza, Italy) using the following parameters: denaturation at 95 °C for 1 min,

annealing at 60 °C for 1 min, and extension at 72 °C for 1 min. The expression of both mouse and rat TRPM8 mRNAs, both presumably expressed in F11 cells, was tested by using specific primers adapted on the known mouse TRPM8 specific primers (sense: 5'-ACA-GACGTGTCTACAGTGA-3'; reverse: 5'-GCTCTGGGCATAACCA-CACTT-3'; <http://pga.mgh.harvard.edu/primerbank/>). In detail, while the TRPM8 sense primer sequence was complementary with the TRPM8 mRNAs of both species, in order to obtain a reverse primer sequence complementary with rat TRPM8 mRNA, it was necessary to remove the last nucleotide from the above mentioned sequence. GAPDH expression was used as internal control. PCR products were analyzed by gel electrophoresis and visualized by using ethidium bromide staining.

Quantitative real-time PCR was carried out in an Eppendorf Mastercycler[®]eprealplex Thermal Cyclers with the TRPM8 primers by using SYBR Green detection. Samples were amplified simultaneously in triplicate in one-assay run, and the *ct* (threshold cycle) value for each experimental group was determined. Data normalization was performed by using the *ct* for the amplification of GAPDH mRNA. Differences in mRNA content between groups were calculated as normalized values by using the 2^{-ΔΔ_{ct}} formula [39].

4.3.3. Calcium imaging experiments

Differentiated F11 cells plated on glass coverslips were incubated with 3 μM Fura-2 acetoxy-methyl ester (Fura-2 AM) for 1 h at room temperature in darkness in a standard Normal Krebs's solution, containing (in mM): NaCl 160, KCl 5.5, CaCl₂ 1.5, MgSO₄ 1.2, HEPES 10, glucose 10, pH 7.4 adjusted with NaOH. Fluorescence images, taken at both 340 nm and 380 nm excitation wavelengths, were obtained by means of a monochromator-based imaging system consisting of a DeltaRAMX[™] Microscope Illuminator (Optical Building Blocks Corporation, Birmingham, NJ) and a coolSNAP ES camera (Princeton Instruments, Trenton, NJ) connected to an inverted microscope (DM IRB, Leica, Wetzlar, Germany) equipped with an oil immersion objective (HCX PL APO, 40×/1.25, Leica). After correction for background fluorescence, the ratio of the fluorescence intensity of images taken at both 340 nm and 380 nm excitation wavelengths every 3 s was calculated. Calibrated ratios were displayed online using MetaFluor Imaging System software (Molecular Devices Corporation, Downingtown, PA).

4.3.4. In vivo tests

Male Swiss CD1 mice weighing 30–35 g were purchased from Harlan (Udine, Italy). They were housed in cages in a room kept at 22 ± 1 °C and with 12/12-h light/dark cycle. The animals were acclimated to their environment for 1 week, and had *ad libitum* access to tap water and standard rodent chow. Animal care was in compliance with Italian (D.M. 116192) and European Economic Community regulations (O.J. of E.C. L 358/1 12/18/1986) for animals used for scientific purposes. Sciatic nerve ligation was performed following the method of Bennett and Xie [40] modified for mice [41]. Briefly, mice were first anesthetized with xylazine (10 mg/kg i.p.) and ketamine (100 mg/kg i.p.), the left thigh was shaved and scrubbed with Betadine, and a small incision (2 cm in length) was made in the middle of the left thigh to expose the sciatic nerve. The nerve was loosely ligated at two distinct sites (spaced at a 2-mm interval) around the entire diameter of the nerve using silk sutures (7–0). The surgical area was closed and finally scrubbed with Betadine. The animals were placed under a heat lamp until they awakened. L-menthol (M), as well as compounds **1a–d** and **1f**, were dissolved in absolute ethanol at a final concentration of 20% w/v. 14 days after Chronic Constriction Injury (CCI) 50 μl of solutions containing these compounds were applied on operated paw at each experimental group (*n* = 6 for each experimental group). Control group (V) was only treated with absolute ethanol. After 20 min

from topical application of tested drugs, a drop (25 μ l) of acetone was applied to the dorsal surface of the ligated paw with a syringe connected to a thin polyethylene tube while the mice were standing on a metal mesh, in order to evaluate cold allodynia. In particular, a brisk foot withdrawal response was considered as a sign of cold allodynia and expressed as cold responses. Three measures of 2 min every approximately 5 min were done. The results measured in each group were expressed both as full time, when the values obtained in all the experimental procedure were measured, and as time-course, when the values obtained during the first, the second and the third phase of each experiment were separately expressed.

4.4. Computational methods

The ligands were simulated considering their neutral forms since they are the favored ones at the physiological pH. After a preliminary optimization using the PM6 semi-empirical method, as implemented in MOPAC 2009, to discard high energy geometries and to calculate precise atomic charges, the conformational behavior of the compounds was investigated using VEGAZZ by a clustered Monte Carlo procedure which generated 1000 conformers by randomly rotating the rotors. All geometries obtained were stored and optimized to avoid high-energy rotamers. For each ligand, the lowest energy structure was then exploited in the docking simulations performed by AutoDock 4.0 using the TRPM8 model recently obtained by homology techniques [23]. In detail, the calculations involved a single TRPM8 monomer and the grid box was set to include all residues within a 15 Å radius sphere around Y745, whose role in ligand recognition has been confirmed by mutational studies [32], in order to comprise the entire binding cavity. The resolution of the grid was $68 \times 77 \times 100$ points with a grid spacing of 0.450 Å. For docking simulations, the flexible bonds of the ligand were left free to rotate to account for ligand flexibility within the binding cavity. Each substrate was docked by using the Lamarckian algorithm as implemented in AutoDock. The genetic-based algorithm ran 30 simulations per substrate with 2,000,000 energy evaluations and up to 27,000 generations. The crossover rate was increased to 0.8, and the number of individuals in each population to 150. All other parameters were left at the AutoDock default settings. The best complexes were finally minimized to favor the mutual adaptability between ligand and receptor and the optimized complexes were then used to re-calculate AutoDock docking scores, VEGA energy scores and X Score values. All mentioned minimizations were performed using the conjugated gradients algorithm as implemented in the Namd 2.51 package with the force-field CHARMM v22 and Gasteiger's atomic charges.

4.5. Statistical analysis

Data are expressed as the mean \pm SEM. The analysis of the data obtained from *in vitro* experiments was performed using GraphPad Prism (GraphPad Software Inc., San Diego, CA). Statistically significant differences between two sets of data were evaluated with the Student's *t* test ($p < 0.05$). Statistical comparisons between multiple (>2) experimental groups was performed by use of the one-way analysis of variance (ANOVA), followed by Newman–Keuls test. Values with a $p < 0.05$ was considered statistically significant.

Appendix A. Supplementary data

Supplementary data related to this article can be found at <http://dx.doi.org/10.1016/j.ejmech.2013.08.056>.

References

- [1] C. Sprengell, Hippocrates: the Aphorisms of Hippocrates, and the Sentences of Celsus; with Explanations and References to the Most Considerable Writers to Which Are Added, Aphorisms upon Several Distempers, Not Well Distinguished by the Ancients, second ed., Sine Nomine, London, 1735.
- [2] R.E. Siegel, Galen on Sense Perception: His Doctrines, Observations and Experiments on Vision, Hearing, Smell, Taste, Touch and Pain, and Their Historical Sources, Karger, Basel, 1970.
- [3] G. Bini, G. Cruccu, K.E. Hagbarth, W. Schady, E. Torebjörk, Analgesic effect of vibration and cooling on pain induced by intraneural electrical stimulation, *Pain* 18 (1984) 239–248.
- [4] J. Sauls, Efficacy of cold for pain: fact or fallacy? *Online J. Knowl. Synth. Nurs.* 6 (1999) 103–111.
- [5] D.D. McKemy, How cold is it? TRPM8 and TRPA1 in the molecular logic of cold sensation, *Mol. Pain* 1 (2005) 16–22.
- [6] A.M. Peier, A. Moqrich, A.C. Hergarden, A.J. Reeve, D.A. Andersson, G.M. Story, T.J. Earley, I. Dragoni, P. McIntyre, S. Bevan, A. Patapoutian, A Trp channel that senses cold stimuli and menthol, *Cell* 108 (5) (2002) 705–715.
- [7] D.D. McKemy, W.M. Neuhauser, D. Julius, Identification of a cold receptor reveals a general role for TRP channels in thermosensation, *Nature* 416 (6876) (2002) 52–58.
- [8] G. Reid, A. Babes, F. Pluteanu, A cold- and menthol-activated current in rat dorsal root ganglion neurones: properties and role in cold transduction, *J. Physiol.* 545 (2002) 595–614.
- [9] C.J. Proudfoot, E.M. Garry, D.F. Cottrell, R. Rosie, H. Anderson, D.C. Robertson, S.M. Fleetwood-Walker, R. Mitchell, Analgesia mediated by the TRPM8 cold receptor in chronic neuropathic pain, *Curr. Biol.* 16 (16) (2006) 1591–1605.
- [10] G. Wasner, J. Schattschneider, A. Binder, R. Baron, Topical menthol – a human model for cold pain by activation and sensitization of C nociceptors, *Brain* 127 (2004) 1159–1171.
- [11] B. Namer, F. Seifert, H.O. Handwerker, C. Maihöfner, TRPA1 and TRPM8 activation in humans: effects of cinnamaldehyde and menthol, *Neuroreport* 16 (9) (2005) 955–959.
- [12] D.D. McKemy, Therapeutic potential of TRPM8 modulators, *Open Access Drug Discovery J.* 2 (2010) 80–87.
- [13] A. Dhaka, A.N. Murray, J. Mathur, T.J. Earley, M.J. Petrus, A. Patapoutian, TRPM8 is required for cold sensation in mice, *Neuron* 54 (3) (2007) 371–378.
- [14] R.W. Colburn, M.L. Lubin, D.J. Stone Jr., Y. Wang, D. Lawrence, M.R. D'Andrea, M.R. Brandt, Y. Liu, C.M. Flores, N. Qin, Attenuated cold sensitivity in TRPM8 null mice, *Neuron* 54 (3) (2007) 379–386.
- [15] L. Zhang, G.J. Barritt, Evidence that TRPM8 is an androgen-dependent Ca^{2+} channel required for the survival of prostate cancer cells, *Cancer Res.* 64 (2004) 8365–8373.
- [16] A.J. Foster, C.P.E. Van Der Logt, W. Erwin, Tetrahydropyrimidine-2-one derivatives and their uses, Unilever plc, WO 2004026840, 2004.
- [17] A. Bassoli, G. Borghonovo, G. Busnelli, G. Morini, Synthesis of a new family of N-aryl lactams active on chemesthesis and taste, *Eur. J. Org. Chem.* 7 (2006) 1656–1663.
- [18] R.R. Calvo, S.K. Meegalla, M.R. Player, Benzimidazole derivatives useful as TRPM8 receptor modulators, Janssenpharmaceutica, N.V., WO 2010132247, 2010.
- [19] N.R. Irlapatil, A. Thomas, D.K. Kurhe, S.Y. Shelke, N. Khairatkar Joshi, S. Viswanadha, I. Mukhopadhyay, Fused oxazole and thiazole derivatives as TRPM8 modulators, Glen-Mark Pharmaceuticals, SA, WO 2010010435, 2010.
- [20] N. Murugesan, Z. Gu, S. Spengel, M. Young, P. Chen, A. Mathur, L. Leith, M. Hermsmeier, E.C. Liu, R. Zhang, E. Bird, T. Waldron, A. Marino, B. Koplowitz, W.G. Humphreys, S. Chong, R.A. Morrison, M.L. Webb, S. Moreland, N. Trippodo, J.C. Barrish, Biphenylsulfonamide endothelin receptor antagonists. 4. Discovery of *N*-[[2'-[[[4,5-dimethyl-3-isoxazolyl]amino]sulfonyl]-4-(2-oxazolyl)]1,1'-biphenyl]-2-yl]methyl]-*N*,3,3-trimethylbutanamide (BMS-207940), a highly potent and orally active ET(A) selective antagonist, *J. Med. Chem.* 46 (1) (2003) 125–137.
- [21] A. Amano, Cooling and pungent agents, *J. Jap. Soc. Cut. Health* 17 (1984) 77–86.
- [22] H.R. Watson, R. Hems, D.G. Rosweel, D.J. Spring, New compounds with the menthol cooling effect, *J. Soc. Cosmet. Chem.* 9 (1978) 185–200.
- [23] A. Pedretti, C. Marconi, I. Bettinelli, G. Vistoli, Comparative modeling of the quaternary structure for the human TRPM8 channel and analysis of its binding features, *Biochim. Biophys. Acta* 1788 (5) (2009) 973–982.
- [24] D. Platika, M.H. Boulos, L. Baizer, M.C. Fishman, Neuronal traits of clonal cell lines derived by fusion of dorsal root ganglia neurons with neuroblastoma cells, *Proc. Natl. Acad. Sci. U. S. A.* 82 (10) (1985) 3499–3503.
- [25] S.F. Fan, K.F. Shen, M.A. Scheideler, S.M. Crain, F11 neuroblastoma x DRG neuron hybrid cells express inhibitory mu- and delta-opioid receptors which increase voltage-dependent K^{+} currents upon activation, *Brain Res.* 590 (1992) 329–333.
- [26] H.H. Chuang, W.M. Neuhauser, D. Julius, The super-cooling agent icilin reveals a mechanism of coincidence detection by a temperature-sensitive TRP channel, *Neuron* 43 (6) (2004) 859–869.
- [27] H.J. Behrendt, T. Germann, C. Gillen, H. Hatt, R. Jostock, Characterization of the mouse cold-menthol receptor TRPM8 and vanilloid receptor type-1 VR1 using a fluorometric imaging plate reader (FLIPR) assay, *Br. J. Pharmacol.* 141 (4) (2004) 737–745.

- [28] R. Madrid, T. Donovan-Rodríguez, V. Meseguer, M.C. Acosta, C. Belmonte, F. Viana, Contribution of TRPM8 channels to cold transduction in primary sensory neurons and peripheral nerve terminals, *J. Neurosci.* 26 (48) (2006) 12512–12525.
- [29] A. Pedretti, M. Labozzetta, A.R. Lo Monte, A. Beccari, A. Moriconi, G. Vistoli, Exploring the activation mechanism of TRPM8 channel by targeted MD simulations, *Biochem. Biophys. Res. Commun.* 414 (1) (2011) 14–19.
- [30] J.S. Walczak, P. Beaulieu, Comparison of three models of neuropathic pain in mice using a new method to assess cold allodynia: the double plate technique, *Neurosci. Lett.* 399 (3) (2006) 240–244.
- [31] K. Vissers, T. Meert, A behavioral and pharmacological validation of the acetone spray test in gerbils with a chronic constriction injury, *Anesth. Analg.* 101 (2) (2005) 457–464.
- [32] H. Xing, M. Chen, J. Ling, W. Tan, J.G. Gu, TRPM8 mechanism of cold allodynia after chronic nerve injury, *J. Neurosci.* 27 (50) (2007) 13680–13690.
- [33] O. Caspani, S. Zurborg, D. Labuz, P.A. Heppenstall, The contribution of TRPM8 and TRPA1 channels to cold allodynia and neuropathic pain, *PLoS One* 4 (10) (2009) e7383.
- [34] M. Bandell, A.E. Dubin, M.J. Petrus, A. Orth, J. Mathur, S.W. Hwang, A. Patapoutian, High-throughput random mutagenesis screen reveals TRPM8 residues specifically required for activation by menthol, *Nat. Neurosci.* 9 (4) (2006) 493–500.
- [35] S. Mandadi, B.D. Roufogalis, ThermoTRP channels in nociceptors: taking a lead from capsaicin receptor TRPV1, *Curr. Neuropharmacol.* 6 (1) (2008) 21–38.
- [36] R. Pan, Y. Tian, R. Gao, H. Li, X. Zhao, J.E. Barrett, H. Hu, Central mechanisms of menthol-induced analgesia, *J. Pharmacol. Exp. Ther.* 343 (3) (2012) 661–672.
- [37] R. Eligeti, S.R. ReddyAtthunuri, R. Samala, F.P. Shaik, G. ReddyKundur, A fast and highly efficient protocol for reductive amination of aromatic aldehydes using NaBH₄ and isoxazoleamines in a ionic liquid medium, *Chin. J. Chem.* 29 (4) (2011) 769–772.
- [38] P. Ambrosino, M.V. Soldovieri, C. Russo, M. Tagliatalata, Activation and desensitization of TRPV1 channels in sensory neurons by the PPAR α agonist palmitoylethanolamide, *Br. J. Pharmacol.* 168 (6) (2013) 1430–1444.
- [39] F.A. Iannotti, E. Panza, V. Barrese, D. Viggiano, M.V. Soldovieri, M. Tagliatalata, Expression, localization, and pharmacological role of Kv7 potassium channels in skeletal muscle proliferation, differentiation, and survival after myotoxic insults, *J. Pharmacol. Exp. Ther.* 332 (3) (2010) 811–820.
- [40] G.J. Bennett, Y.K. Xie, A peripheral mononeuropathy in rat that produces disorders of pain sensation like those seen in man, *Pain* 33 (1) (2008) 87–107.
- [41] R. Russo, J. LoVerme, G. La Rana, T.R. Crompton, J. Parrott, A. Duranti, A. Tontini, M. Mor, G. Tarzia, A. Calignano, D. Piomelli, The fatty acid amide hydrolase inhibitor URB597 (cyclohexylcarbamic acid 3'-carbamoylbiphenyl-3-yl ester) reduces neuropathic pain after oral administration in mice, *J. Pharmacol. Exp. Ther.* 322 (1) (2007) 236–242.